

Phase diagrams of the extended Bose-Hubbard model in one dimension by Monte-Carlo simulation with the help of a stochastic-series expansion

Keima Kawaki, Yoshihito Kuno, and Ikuo Ichinose

Department of Applied Physics, Nagoya Institute of Technology, Nagoya 466-8555, Japan

(Received 11 May 2016; revised manuscript received 13 April 2017; published 1 May 2017)

In this paper, we study phase diagrams of the extended Bose-Hubbard model (EBHM) in one dimension by means of the quantum Monte-Carlo (QMC) simulation using the stochastic-series expansion (SSE). In the EBHM, there exists a nearest-neighbor repulsion as well as the on-site repulsion. In the SSE-QMC simulation, the highest particle number at each site, n_c , is also a controllable parameter, and we found that the phase diagrams depend on the value of n_c . It is shown that in addition to the Mott insulator, superfluid, density wave, the phase so-called Haldane insulator, and supersolid appear in the phase diagrams, and their locations in the phase diagrams are clarified.

DOI: [10.1103/PhysRevB.95.195101](https://doi.org/10.1103/PhysRevB.95.195101)

I. INTRODUCTION

Quantum many-body systems in one spatial dimension (1D) have strong fluctuations compared with higher-dimensional systems, and as a result, they sometimes have exotic quantum phases and nontrivial phase diagrams that cannot be obtained by mean-field theories. Recently, experiments on ultracold atomic systems can produce controllable and versatile strongly-correlated systems on an optical lattice [1]. There, the strong correlations mean large on-site and off-site atomic interactions [2], a strong artificial magnetic field [3], geometrical frustrations, e.g., on triangular and honeycomb lattices [4], etc. In this paper, the phase diagram of an extended Bose-Hubbard model (EBHM) on the 1D lattice is investigated by means of one of the most reliable numerical methods, i.e., the quantum Monte-Carlo (QMC) simulation with the stochastic-series expansion (SSE) [5].

This model is expected to have a rich phase diagram due to large fluctuations and nearest-neighbor interactions. It is believed that the model has similar properties of spin chain models, which are important models in condensed matter physics. The previous studies [6] discussed that in the case of the strong on-site interaction, the particle number at each site is restricted to be less than two, and as a result, the three body constraint, $(a^\dagger)^3 = 0$, seems to appear [7–10]. Under this constraint, the EBHM can be mapped to a spin-1 *XXZ*-type model by using the Holstein-Primakoff transformation [6,11]. From this relationship between the EBHM and quantum spin model, one may expect the existence of an interesting phase, i.e., Haldane insulator (HI), which is similar to the Haldane phase in the quantum spin system [12,13]. So far, a number of the numerical studies [14–16] investigated the phase diagram of the EBHM in the canonical ensemble incorporating the constraint $(a^\dagger)^3 = 0$. In most of these studies, the filling fraction is fixed to unity, although some of them studied other low-filling cases. Furthermore, we expect that real experimental set up may relax such a three body constraint, then the mapping of the EBHM to the spin-1 model is not necessarily applicable. Therefore, the EBHM may have a richer phase diagram than the spin model. In particular, the detailed phase diagram of the EBHM in the grand-canonical ensemble is not completely understood yet.

In this paper, we consider the grand-canonical ensemble of the EBHM and study the phase diagram by the SSE-QMC simulations. In fact, the SSE-QMC simulation is suitable for the study on the grand-canonical ensemble as large system-size calculation is possible due to less memory consumption compared to other numerical methods, e.g., the exact diagonalization method. The obtained phase diagram exhibits various phases with various filling fractions. For example, the aforementioned HI appears not only at the unit filling but also at the half filling.

The paper is organized as follows. In Sec. II, we introduce the EBHM and explain the SSE-QMC simulation. Various quantities to identify phases are introduced. In Sec. III, results of the numerical study are presented. In the practical simulation, the maximum number of particles at each site (n_c) and also the value of the next-nearest-neighbor repulsion (V) are fixed. Phase diagrams in the [on-site repulsion]-[chemical potential (i.e., average particle number)] are obtained. Results show the dependence of the phase diagrams on the value of n_c . System-size dependence of the results are also carefully examined. Section IV is devoted for discussion and conclusion.

II. EXTENDED BOSE-HUBBARD MODEL AND QUANTUM MC SIMULATION WITH SSE

We start with the EBHM defined on a 1D lattice whose Hamiltonian H_{EBH} is given as

$$H_{\text{EBH}} = \sum_a \left[-J(\hat{\psi}_a^\dagger \hat{\psi}_{a+1} + \hat{\psi}_{a+1}^\dagger \hat{\psi}_a) + \frac{U}{2}(\hat{\rho}_a - 1)\hat{\rho}_a + V\hat{\rho}_a\hat{\rho}_{a+1} \right],$$

$$\hat{\rho}_a \equiv \hat{\psi}_a^\dagger \hat{\psi}_a, \quad (1)$$

where $\hat{\psi}_a^\dagger$ and $\hat{\psi}_a$ are creation and annihilation operators of boson at site a , respectively, and $\hat{\rho}_a$ is the number operator. The coefficient J represents the hopping strength, U is the on-site interaction, and $V(> 0)$ is the nearest-neighbor (NN) repulsive interaction generated by, e.g., a dipole-dipole interaction in gases loaded on the optical lattice [17,18]. In the cold atomic gas system, the above on-site repulsion $U(> 0)$ represents the sum of s -wave scattering interaction U_s

and on-site dipole-dipole interaction U_d ; $U = U_s + U_d$. The s -wave scattering amplitude U_s is highly controllable by the Feshbach resonance [19]. In practical experiments, the ratio V/U is highly controllable by using the combination of the Feshbach resonance and selection of species of loaded atoms [2,20].

The global phase diagram of the EBHM in Eq. (1) is important, and we shall clarify the low-filling phase diagram of the EBHM by means of the most reliable numerical method, i.e., the SSE-QMC simulation [5]. In the SSE-QMC simulation, the partition function is expanded as

$$\begin{aligned} Z_{\text{EBH}} &= \text{Tr}(e^{-\beta(H_{\text{EBH}} - \mu N)}) \\ &= \sum_{n=0}^{\infty} \frac{1}{n!} \text{Tr}(-\beta(H_{\text{EBH}} - \mu N))^n, \end{aligned} \quad (2)$$

where $\beta = 1/(k_B T)$, k_B is the Boltzmann constant, T is the temperature, μ is the chemical potential, and $N = \sum_a \hat{\rho}_a$. As we are interested in the ground-state phase diagram, we take $\beta \rightarrow$ large. In the evaluation of Z_{EBH} in Eq. (2), the particle-number eigenstates $\prod_a |\rho_a\rangle$, $\hat{\psi}_a^\dagger \hat{\psi}_a |\rho_a\rangle = \rho_a |\rho_a\rangle$, are employed as a basis of quantum states. Then, the Hamiltonian H_{EBH} is divided into the diagonal part (the U and V terms) and off-diagonal part (the J term), and Eq. (2) is re-expanded in powers of these parts. Weight of each term in the expansion is determined by the MC methods. The trace in Eq. (2) can be calculated by putting intermediate states between the Suzuki-Trotter decomposed Hamiltonians. Here, Monte-Carlo sampling is applied for each decomposed Hamiltonian operator. In the sampling, the loop algorithm [5] allows us to create closed loops of transition states along imaginary time (temperature) direction.

In this paper, we consider the case of low fillings and restrict the Hilbert space $\{|\rho_a\rangle\}$ to $\rho_a = 0, \dots, n_c$ in evaluating Z_{EBH} in Eq. (2), where n_c is the largest particle number at each site. In the practical calculation, we first concentrate on the case $n_c = 2$ and 3, and later on we show results in the case of higher n_c . In Refs. [14–16], the EBHM was studied mostly by the density-matrix renormalization group (DMRG). There, the average particle number per site was fixed to unity, i.e., $\rho = \frac{1}{L} \sum_a \langle \rho_a \rangle = 1$, where L is the system size, and the phase diagram in the $(U-V)$ plane was obtained. In the present study, on the other hand, we employ the grand-canonical ensemble and vary the chemical potential, i.e., the average particle density, to obtain the phase diagrams, although we focus on the low-filling region like $0 < \rho < 3$ at first. As far as we know, the phase diagram of the EBHM in the grand-canonical ensemble is a new result. By studying the EBHM in the grand-canonical ensemble, we found that the model has different phase diagrams depending on the value of n_c . For the case of the unit filling $\rho = 1$ and $n_c = 2$, the phase diagram of the EBHM was obtained by the DMRG methods [21]. As we explain later on, the obtained phase diagrams by the SSE-QMC simulation in the present study are in good agreement with the phase diagram obtained in Ref. [21].

In the practical calculation, we put $\hbar = 1$, $J = 1$ (as the unit of energy), and $\beta = 200$, which corresponds to a very low temperature case [5] and employ the periodic boundary condition. We calculated the average particle density and also

order parameters as varying the chemical potential μ for fixed values of U and V .

Before going into the study on the EBHM, we investigated the phase diagram of the standard Bose Hubbard model *without* the NN repulsion, i.e., the $V = 0$ case. The results support the accuracy of our numerical code because the well-established phase diagram of the Bose-Hubbard model was reproduced quite accurately.

To distinguish the phases, we measure various order parameters. The superfluid (SF) order parameter ρ_s is related to the winding number of the boson world lines and defined as [22,23]

$$\rho_s = \frac{1}{2\beta L} \langle (N^+ - N^-)^2 \rangle, \quad (3)$$

where $N^+(N^-)$ is the total number of the hopping term in the positive (negative) direction that appears in the MC simulation. In the practical calculation of ρ_s in Eq. (3), we take the average of all 1D spatial configurations appearing in the 2D plain of the 1D space and the expansion step of the completed loop. For the 1D EBHM at large fillings, detailed path-integral MC simulations were performed in Ref. [24], and the Mott insulator (MI) \leftrightarrow SF phase transition is observed as a Kosterlitz-Thouless transition.

Other order parameters that identify the density wave (DW) and the HI are the following,

$$G_{\text{DW}}(\ell) = (-1)^\ell \langle \delta\rho_{a+\ell} \delta\rho_a \rangle, \quad (4)$$

$$G_{\text{string}}(\ell) = \langle \delta\rho_{a+\ell} e^{i\pi \sum_{a \leq k < a+\ell} \delta\rho_k} \delta\rho_a \rangle, \quad (5)$$

where $\delta\rho_a \equiv \rho_a - \rho$. $G_{\text{DW}}(\ell)$ is a DW correlation function to detect the DW phase. On the other hand $G_{\text{string}}(\ell)$ is a string-order correlation function, which can identify the HI phase. (The definition of this correlation function is slightly different from that used in the previous studies in Refs. [14–16], i.e., in the definition $\delta\rho_a = \rho_a - \rho$, we do not fix the average density ρ to unity as we employ the grand-canonical ensemble.) A finite value of $\lim_{\ell \rightarrow \infty} G_{\text{DW}}(\ell)$ shows the existence of the DW, which is expected to form for large V . Finally, a finite value of $\lim_{\ell \rightarrow \infty} G_{\text{string}}(\ell)$ and the *vanishing DW order* mean that the corresponding state is the HI. This order is similar to the Haldane order in the antiferromagnetic (AF) spin chain, and a typical configuration in the HI is shown in Ref. [11]. On the other hand, the nonvanishing DW order always accompanies a finite string order.

III. NUMERICAL RESULTS

A. Phase diagrams for $n_c = 2$ and 3

We first show the results of the $V = 2.0$ case with the system size $L = 32$. Obtained phase diagrams are shown in Fig. 1 for the $n_c = 2$ and $n_c = 3$ cases. There are four phases; the MI with $\rho = 1$ ($n_c = 2$) and $\rho = 1.5$ ($n_c = 3$), SF, DW, and the HI. For the $n_c = 2$ case, the DW has the $|\dots, 2, 0, 2, 0, \dots\rangle$ configuration and the HI forms in a relatively large- U region, in which a holon exists between every two doublons as indicated by the finite $G_{\text{string}}(\ell)$ [11]. It should be remarked that the $n_c = 2$ EBHM is closely related to the spin-1 quantum Heisenberg spin chain [11,13]. The HI corresponds to the Haldane phase in

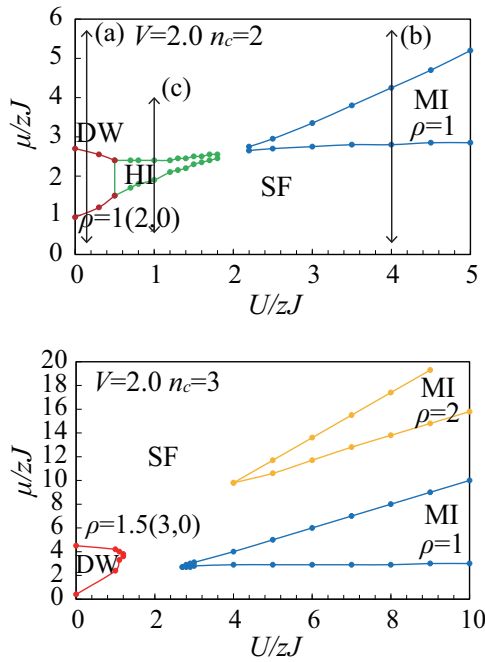


FIG. 1. Phase diagram of the EBHM obtained by the SSE-QMC simulations for $V = 2.0$ and $n_c = 2$ ($n_c = 3$) in the upper (lower) plane. There are SF (superfluid), MIs (Mott insulators), DWs (density waves), and HI (Haldane insulator). In the case of $n_c = 2$ and at unit filling $\rho = 1$, a direct transition from the MI to HI does not take place, instead, there is the tiny SF region. z is the number of the NN sites and in the present case $z = 2$.

the spin system. On the other hand for the case $n_c = 3$, the DW with $\rho = 1.5$ appears and the $|\dots, 3, 0, 3, 0, \dots\rangle$ configuration is realized there, whereas the HI does not form. We have not found the DW with $\rho = 1$ in the $(U/J - \mu/J)$ plane in the present grand-canonical ensemble calculation, although we searched it in the low μ/J region.

Typical behaviors of the order parameters are shown in Fig. 2. We also calculated the order parameters for the system sizes $L = 40$ and 48 and verified that the phase boundaries are stable. In the MI and DW phases, the SF density is very low. On the other hand, there exists a small but finite SF in the HI. Later on, we shall show that the finite SF in the HI is a finite-size effect. [More detailed analysis of the finite-size effect will be given after showing the results of $V = 4.0$.]

As Fig. 2(c) shows, the string order $G_{\text{string}}(\ell)$ exhibits curious fluctuations in the SF that might stem from the relatively large density fluctuations, and these fluctuations have small but finite spatial correlations. This unexpected behavior of $G_{\text{string}}(\ell)$ becomes clearer in the case of $V = 4.0$ that we shall study shortly. We shall discuss the small but somewhat periodic regions with a finite $G_{\text{string}}(\ell)$ after showing the phase diagrams of the $V = 4.0$ case.

Next we show the phase diagram for $V = 3.0$ in Fig. 3. Features of the phase diagrams are almost the same as that in the case of $V = 2.0$, but the region of the HI is getting smaller compared to the case of $V = 2.0$. Furthermore in the phase diagram of $V = 3.0$ with $n_c = 2$, in the vicinity of the DW, there exists a state that we call quasisupersolid (qSS). We shall discuss this state shortly.

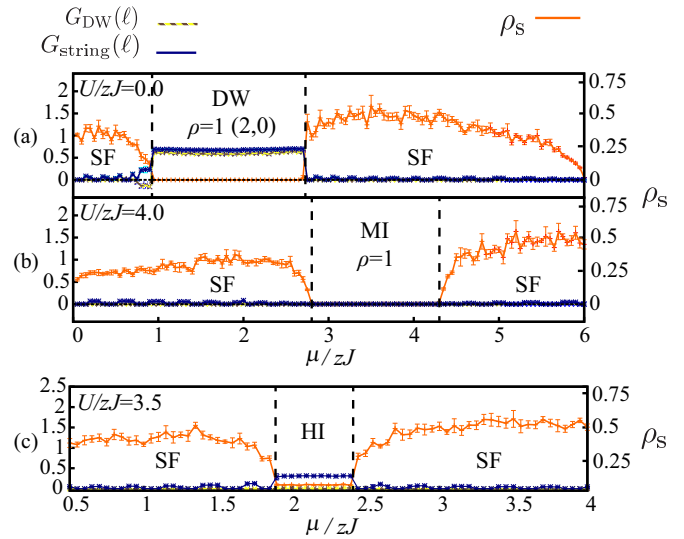


FIG. 2. Various order parameters for $n_c = 2$ and $V = 2.0$ as a function of μ/zJ . (a) Results for $U/zJ = 0.0$. (b) $U/zJ = 4.0$. (c) $U/zJ = 1.0$.

Finally we show the phase diagram of the $V = 4.0$ case in Fig. 4. In the case of $n_c = 2$, there exists a small HI between the MI and DW for $\rho = 1$. Behavior of the order parameters used to obtain the phase diagram for $V = 4.0$ with $n_c = 2$ are shown in Fig. 5. On the other hand for $n_c = 3$, the phase diagram is rather complicated, i.e., the supersolid (SS) forms between two DWs with $\rho = 1$ and $\rho = 1.5$. In

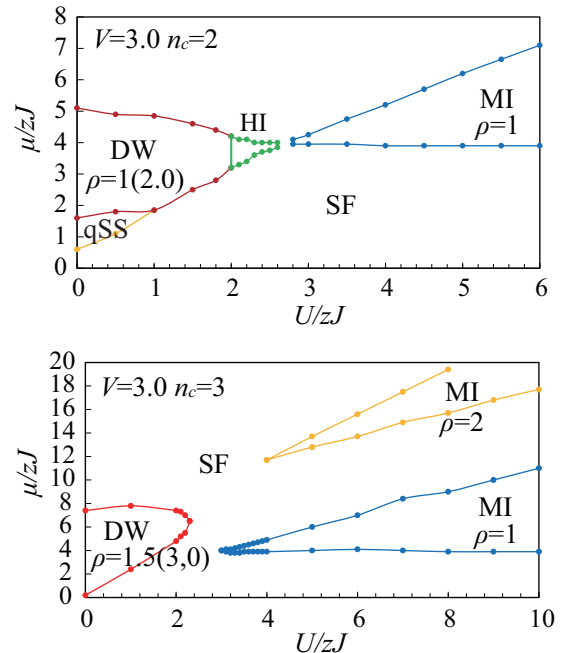


FIG. 3. Phase diagram of the EBHM obtained by the SSE-QMC simulations for $V = 3.0$ and $n_c = 2$ ($n_c = 3$) in the upper (lower) plane. There are SF, MIs, DWs, and HI as in the case of $V = 2.0$. In addition in the case $n_c = 2$, there appears a phase that we call quasisupersolid (qSS). For details, see Fig. 8. As in the case of $V = 2.0$ and $n_c = 2$, the tiny SF region exists between the MI and HI at unit filling $\rho = 1$.

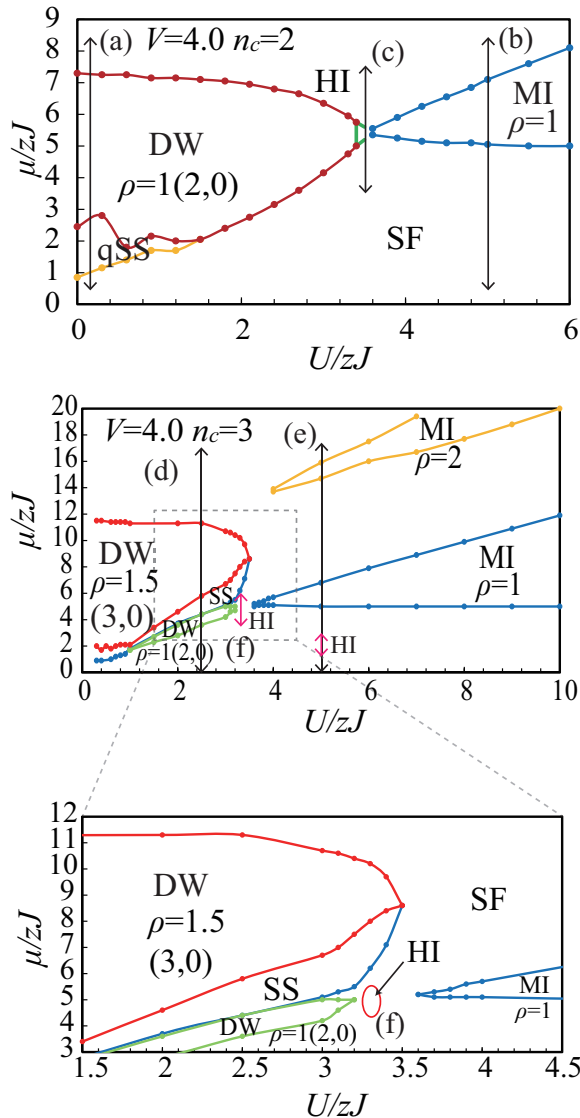


FIG. 4. Phase diagram of the EBHM obtained by the SSE-QMC simulations for $V = 4.0$ and $n_c = 2$ ($n_c = 3$) in the upper (lower) plane. There are SF, MIs, DWs, and HI. qSS stands for the quasisupersolid with a finite SF. The phase diagram of $n_c = 3$ is rather complicated compared to the case of $n_c = 2$. In addition to the $\rho = 1$ HI, there exists the $\rho = \frac{1}{2}$ HI, which is discussed in Sec. IV.

the SS, a DW-like inhomogeneous state is realized, and the average particle number is fractional $1 < \rho < 1.5$. Particles (holes) move rather freely on the base of the $\rho = 1$ ($\rho = 1.5$) DW and as a result, the SF appears. Interestingly enough, the phase diagram also indicates the existence of the $\rho = \frac{1}{2}$ HI as the order parameters in Fig. 6 show. We shall discuss this HI in Sec. IV.

The calculations of the string order in Figs. 5(c), 6(e), and 6(f) exhibit rather curious behavior. It has a nonvanishing value in specific parameter regions of μ/zJ , which have a shelllike structure. Figure 7 is a blow up of Fig. 6(f). We show the density as a function of the chemical potential and find the step-wise behavior of the density synchronizing with the string order. This result exhibits that a state with a finite string order forms in the system with an even number of particles although

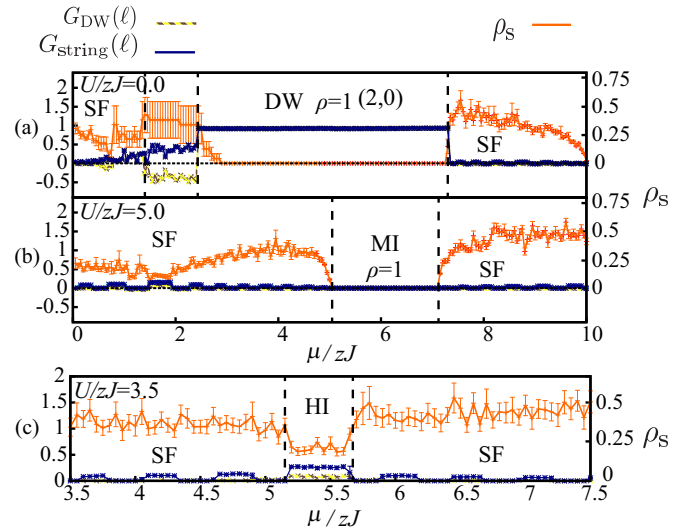


FIG. 5. Typical correlation functions in the $n_c = 2$ and $V = 4.0$ phase diagram in Fig. 4. (a)–(c) correspond to the lines indicated in Fig. 4, respectively. The system size is $L = 32$. In calculating the order parameters Eqs. (4) and (5), we used $\ell = L/2$. SF (superfluid), MI (Mott insulator), DW (density wave), and HI (Haldane insulator).

in some regions no reduction of the SF is observed. This might be a finite-size effect. See later discussion of the “finite-size scaling” analysis of the SF. For example in the system with 34 particles, typical configurations are produced from those of the $\rho = 1$ HI by adding one doublon ($\rho_a = 2$) to the system or replacing a singleton ($\rho_a = 1$) with a triplon ($\rho_a = 3$).

Let us briefly comment on the phase that we call qSS, which exists in the phase diagrams for $n_c = 2$ in Figs. 3 and 4. As the chemical potential decreases, the particle density decreases

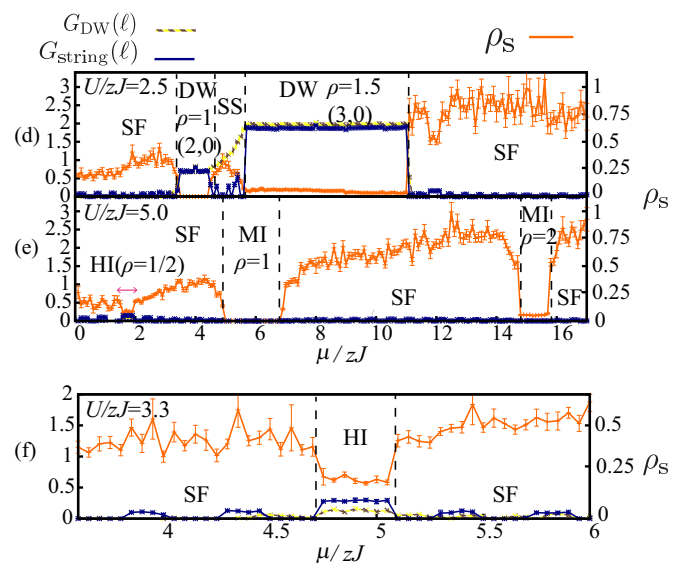


FIG. 6. Typical correlation functions along the line (d)–(f) in the $V = 4.0$ phase diagram in Fig. 4. The system size is $L = 32$. In calculating the order parameters Eqs. (3)–(5), we used $\ell = L/2$. SF (superfluid), MI (Mott insulator), DW (density wave), HI (Haldane insulator), and SS (supersolid). From the results in (e) and (f), we conclude the existence of the HIs at $\rho = \frac{1}{2}$ ($\mu/J \simeq 1.5$) and $\rho = 1$ ($\mu/J \simeq 4.7$).

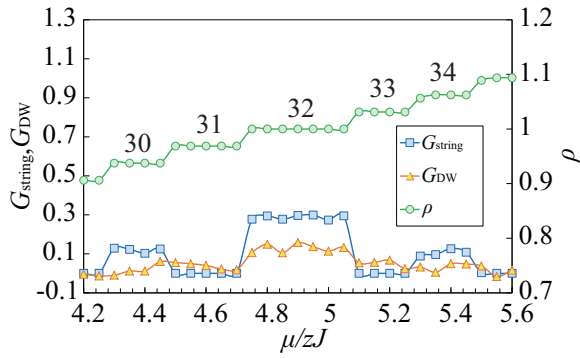


FIG. 7. The string order, the DW, and the density ρ as a function of μ/zJ in the adjacent region of the $\rho = 1$ HI. $L = 32$. The numbers refer to total particle number in the system. Density ρ exhibits a step-wise behavior synchronizing with the string order. The result indicates that a state with a finite string order forms in the system with an even number of particle.

from the $\rho = 1$ DW. As a result of depletion of particles, the DW is divided into a few parts by “domain walls”. A typical configuration of the qSS obtained by the SSE-QMC simulation is shown in Fig. 8. A pair of holes plays a role of a “domain wall”. The SSE-QMC simulation shows that the G_{DW} has negative values. As the system is getting large, pairs of holes (domain walls) are mobile, and as a result this state has a finite SF as seen in Fig. 8. In the large system size limit *with keeping the density of particle constant*, it is expected that the DW order parameter tends to vanish while a small but finite SF remains due to the mobility of domain walls. This is the reason why we call that phase qSS.

We examined the system-size dependence of the HI and MI phase boundaries in Figs. 1, 3, and 4. Figure 9 shows that the phase boundaries obtained by the present SSE-QMC simulation do not have a large system size dependence. In the very vicinity of the tip of the HI phase, we found that the string order gradually loses a step-wise behavior, and simultaneously the very low SF density starts to appear. From these behaviors of the order parameters, a clear phase boundary was not obtained in the present simulation in the very vicinity of the tips of the MI and HI.

We also studied the system-size dependence of the HI with $\rho = 1$, which is observed in Fig. 6(f). We plot $G_{\text{string}}(L/2)$ as a function of $1/L$ in Fig. 10, as a “finite-size scaling” analysis. It is interesting and also important to see a “finite-size scaling” of the SF and DW. See Fig. 10. From these results, it is expected that the finite SF and DW in the $\rho = 1$ HI is a system-size effect. It should be remarked here that while the stochastic Green-function QMC simulation in Ref. [15] exhibits a strong system size dependence of the string order in the HI, the present SSE-QMC simulation does not have such a strong dependence in the string order. The difference may stem from the fact that while the Green-function QMC is applied to the canonical-ensemble system, our SSE QMC is applied to the grand-canonical ensemble.

The phase diagrams in Figs. 1, 3, and 4 should be compared with the results of the previous works in which the average density is fixed, i.e., the canonical ensemble. In Refs. [14,21], by means of the DMRG, the $(U - V)$ phase diagram for the

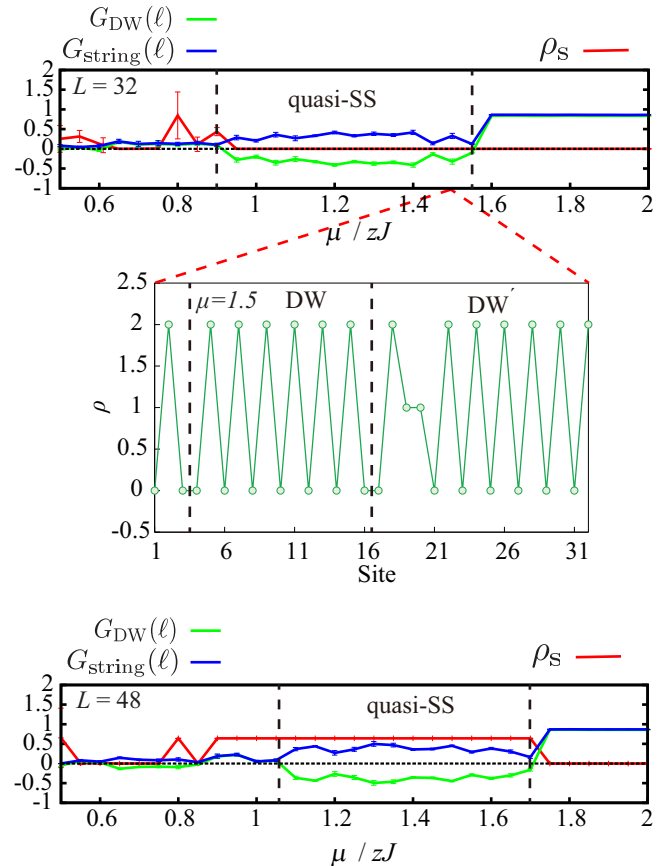


FIG. 8. (Upper panel) Order parameters for the qSS in Fig. 3 with $L = 32$. As the chemical potential decreases, the particle density decreases and extra holes and single occupied sites are generated in the $\rho = 1$ DW existing for $\mu/zJ > 1.6$. Then the DW is divided into smaller DWs, and the order parameter of the DW has negative values. (Middle panel) A typical configuration generated by the MC simulation. (Bottom panel) Order parameters for $L = 48$. Walls dividing DW into smaller ones move under the MC simulations in large system size. As a result, the state has a finite SF density. This is the reason why we call this state qSS.

$\rho = 1$ was obtained. For the case of $n_c = 2$, our results are in good agreement with those in Refs. [14,21]. However, the SF exists between the $\rho = 1$ MI and HI as in Figs. 1 and 3, whereas the SF does not exist there in the phase diagram obtained in Refs. [14,21]. The phase diagram of $V = 4.0$ with $n_c = 3$ in Fig. 3 is in good agreement with that obtained by DMRG in Refs. [14–16] for $\rho = 1$, that is, the phase transitions from the MI, SF, HI, and DW take place as the value of U/J decreases. The other parts of the phase diagrams and the calculations of the order parameters in Figs. 1–6 are new results.

B. Phase diagrams for $V = 2.0$ with $n_c = 4, 5$, and 6

In the previous subsection, we studied the case $n_c = 2$ and 3 and obtained the phase diagrams by calculating various order parameters. In this section, we consider the system with higher n_c . By a simple application of the Holstein-Primakoff transformation for the EBHM with the highest-particle number at each site n_c , the EBHM is mapped into a spin $s = n_c/2$ model. This transformation connecting two models naively

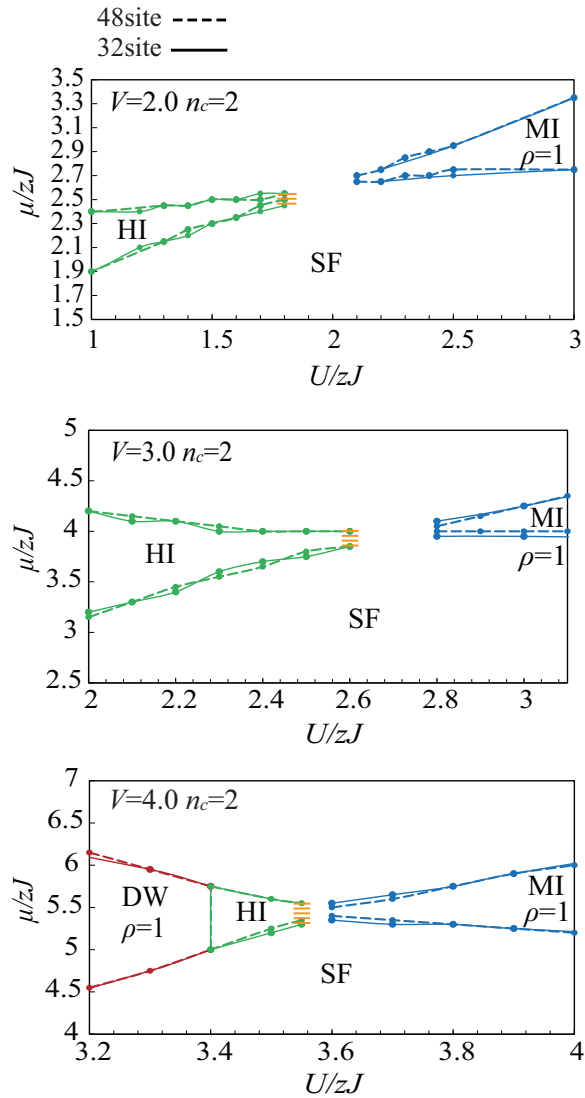


FIG. 9. System-size dependence of the phase boundaries in the case of $n_c = 2$. Simulations of the system sizes $L = 32$ and $L = 48$ exhibit almost the same phase boundaries for all phase transitions. This indicates that the system size $L = 32$ reaches a scaling region of the thermodynamic limit. We have also verified other cases and obtained a similar system-size dependence.

implies that the HI phase appears in the case of an integer s , i.e., an even integer n_c [25]. Strictly speaking, however, the EBHM is not mapped to the simple Heisenberg-type spin model, but to a spin- s model with complicated interactions [26]. Thus, the ground-state phase diagram conjectured by the simple correspondence between the boson and spin models is not necessarily correct. Moreover, the one-dimensional system has strong quantum fluctuations. Thus, the truncation number of the particle in the SSE, n_c , may be an important ingredient to determine the ground-state phase diagram. To this end, we perform the SSE-QMC simulation with higher n_c in this subsection.

The obtained phase diagrams in the $(U/J - \mu/J)$ plain are shown in Fig. 11. The MIs with the density $\rho = 1$ and 2 exist in the phase diagram as in the previous low n_c case. Their location does not change substantially from the case of $n_c = 3$ (and

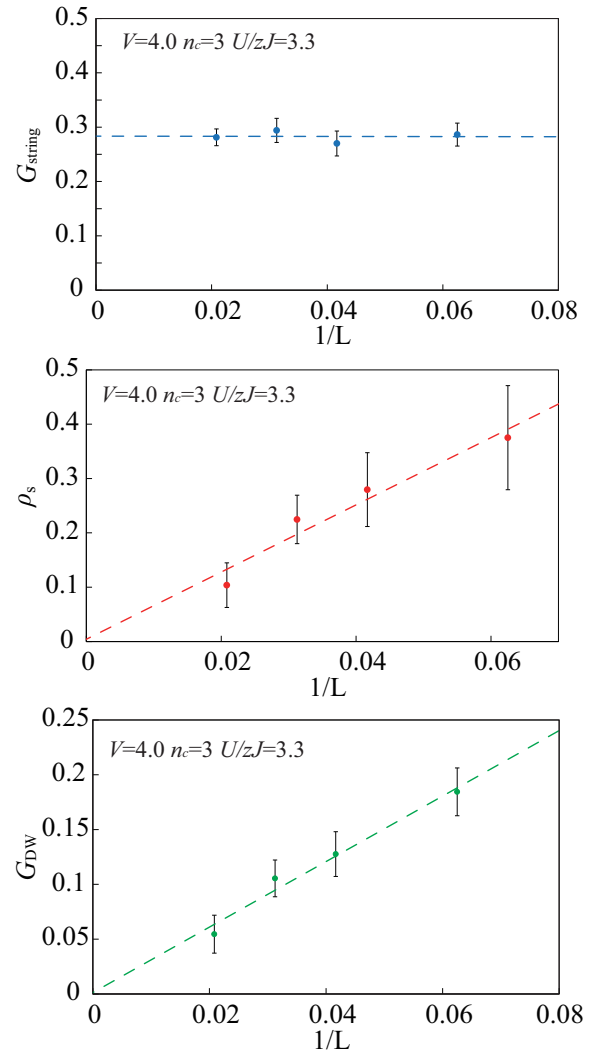


FIG. 10. The string order (upper panel), SF (middle panel), and DW (bottom panel) in the $\rho = 1$ HI as a function of $1/L$. $G_{\text{string}}(L/2)$ has a very weak system-size dependence, whereas ρ_s and DW tend to vanish for $L \rightarrow \infty$.

$n_c = 2$). This result is plausible, as the density fluctuations are small in the MIs. On the other hand for the DW state, ones with the higher average density appear in the $n_c = 4, 5$, and 6 cases, i.e., $\rho = 2.0, 2.5$, and 3, respectively. In the $\rho = 2.0, \rho = 2.5$, and $\rho = 3$ DWs, the state $|\dots, 4, 0, 4, 0, \dots\rangle$, $|\dots, 5, 0, 5, 0, \dots\rangle$, and $|\dots, 6, 0, 6, 0, \dots\rangle$ form. As seen in Fig. 11, the SS also forms between the DW and SF. However, we could not find a HI similarly to the case of $n_c = 3$. For higher n_c , particle number at each site can fluctuate rather freely compared with the case of lower n_c , and as a result, the state with particle number from zero to n_c appears at each site even in the vicinity of the DW. This may be the reason for the nonexistence of the HI. The above numerical results also indicate that even though the system parameters are set around unit filling, the EBHM in the grand-canonical ensemble cannot be directly connected to the spin-1 model because the HI phase does not exist. As a future work, to clarify the above problem, other numerical methods, e.g., the DMRG, exact diagonalization should be applied to the EBHM of higher n_c .

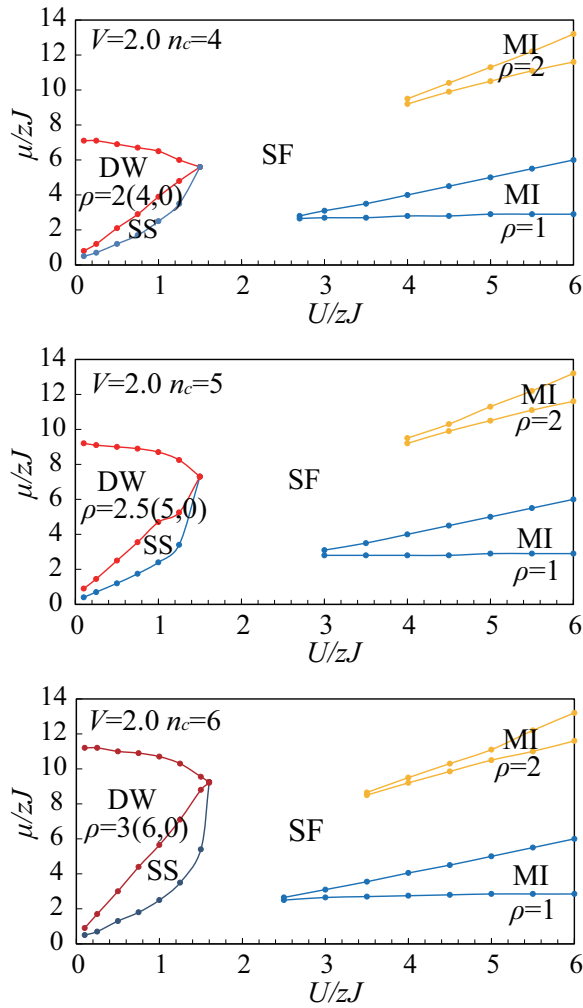


FIG. 11. Phase diagrams for $V = 2.0$, $n_c = 4, 5$, and 6 . Higher-filling MI and DW appear with the SS. This result shows the n_c dependence of the phase diagram.

IV. DISCUSSION AND CONCLUSION

In this work, we studied the phase diagrams of the EBHM with the NN repulsion by means of the SSE-QMC simulations. We considered the grand-canonical ensemble of the system at low fillings and found that the model has a very rich phase diagram. In the present study, the highest particle number at each site, n_c , is a controllable parameter as well as the parameters in the Hamiltonian and the filling factor. Then, we obtained the phase diagrams for the systems without fixing the filling factor. This is in strong contrast with the previous studies, in which the EBHM was investigated in the canonical ensemble with specific fillings and also with a small highest particle number such as $n_c = 2$ and 3 . In this sense, we have obtained the global and detailed phase diagrams compared to those of the previous works.

In the SSE-QMC simulation, the measurement of the order parameters clarifies phase boundaries and clearly exhibits physical properties of each phase, and the phase diagrams have very small system-size dependence. Most of the results are in good agreement with the previous works, which study the EBHM in the canonical ensemble at the unit filling. Besides

the MI, SF, and DW states, there exist the HI and SS. We also found rather strong n_c dependence of the phase diagram. This result seems important for the experimental set up to observe the phases in the 1D EBHM, in particular, the HI.

We used the string order parameter $G_{\text{string}}(L/2)$, defined as in Eq. (5), for searching HIs at various filling factors. For the system of integer fillings, this quantity is often employed and it has a real value, whereas for noninteger fillings, $G_{\text{string}}(L/2)$ can be a complex number. However, our numerical study reveals that it is always real. One may wonder what a finite value of $G_{\text{string}}(L/2)$ physically means for fractional fillings. For the case of the half filling $\rho = 1/2$, the numerically observed positive value of $G_{\text{string}}(L/2)$ indicates that certain specific configurations of the boson are realized there. It is also interesting and important to examine the “finite-size scaling” of $G_{\text{string}}(L/2)$, ρ_s , and $G_{\text{DW}}(L/2)$ for the $\rho = 1/2$ state. The results are shown in Fig. 12. It is obvious that the SF density

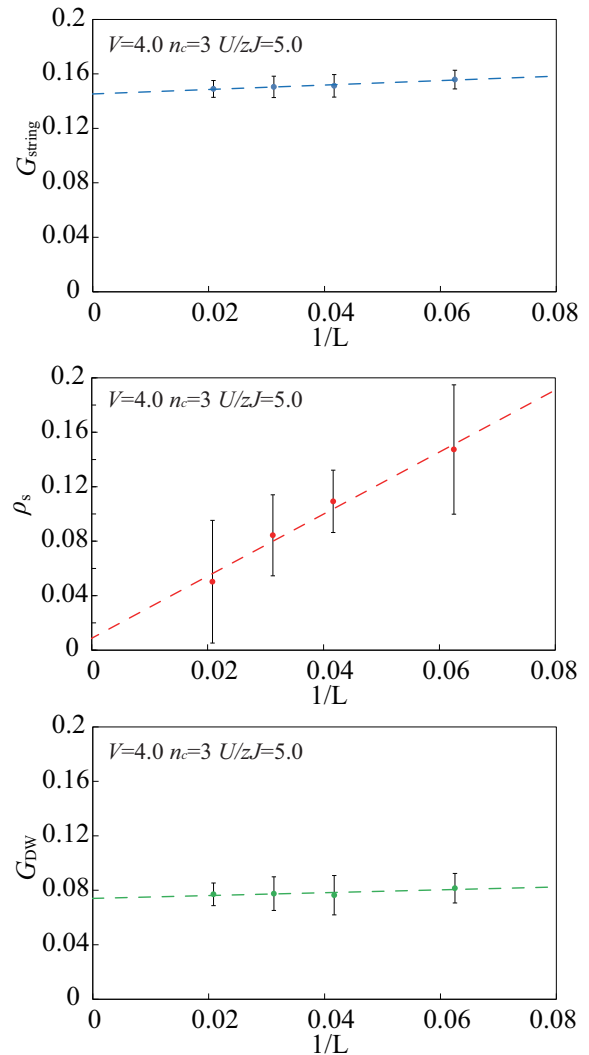


FIG. 12. String order (upper panel), SF (middle panel), and DW (bottom panel) in the $\rho = 1/2$ HI-DW state. SF density tends to vanish for large L . On the other hand, both the string and DW orders have a finite value for large L . However, the string order is larger than the DW order, and this behavior indicates that an unexpected state exists for $\rho = 1/2$, i.e., the HI-DW state.

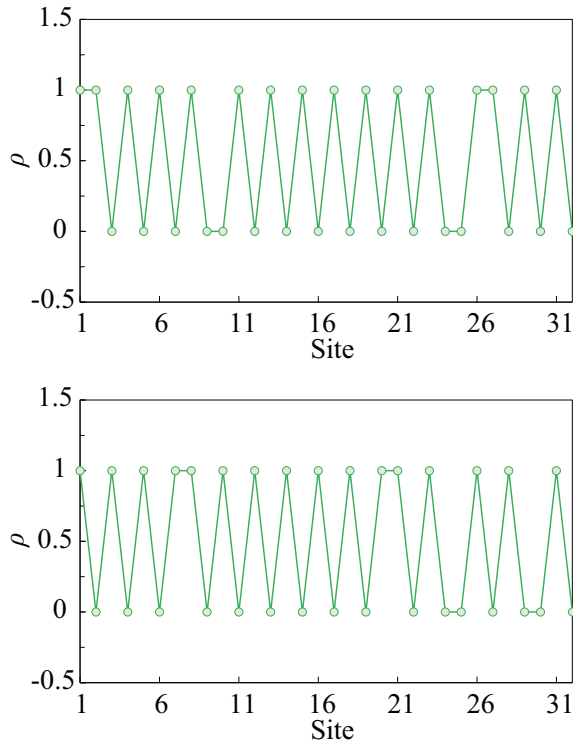


FIG. 13. Typical configurations of the $\rho = 1/2$ HI-DW obtained by the SSE-QMC simulation. In the DW-like background, a local excess of particle is compensated by a pair of holes. Distance between them can be considerably large as the MC simulation indicates. The DW is weakened by these fluctuations.

ρ_s tends to vanish for large L . $G_{\text{string}}(L/2)$ and $G_{\text{DW}}(L/2)$ both keep a finite value for large L , whereas numerically $G_{\text{string}}(L/2) \sim 2 \times G_{\text{DW}}(L/2)$. This strong enhancement of the string order compared with the DW order indicates that the $\rho = 1/2$ state is *not* the genuine DW nor the genuine HI, and we dare to call it $\rho = 1/2$ HI-DW. [As Figs. 5(a) and 6(d) show, $G_{\text{string}}(L/2) \simeq G_{\text{DW}}(L/2)$ in the DW.] Snapshots obtained in the SSE-QMC simulations are shown in Fig. 13. In the DW-like background, a local excess of particle is compensated by a pair of holes, and the DW is weakened by these fluctuations

as distances between a particle pair and a hole pair can be considerably large. The HI-DW may connect with the $\rho = 1/2$ DW via a phase transition or a crossover as the NN repulsion V increases.

We have recognized that $G_{\text{string}}(L/2)$ always has a non-negative real value at other fractional fillings. This seems to indicate that certain chosen configurations are realized in the states with $G_{\text{string}}(L/2) > 0$. This problem is under study.

In recent papers, we pointed out that some parameter regions of the EBHM are regarded as a candidate for the quantum simulator of a gauge-Higgs model on a lattice [24]. This observation is quite important as the dynamical properties of the lattice gauge theory is a very difficult problem and the quantum simulation using ultracold atomic gases can study the time evolution of the system. It is also important to see how exotic states of the EBHM, e.g., the HI, are understood from the gauge-theoretical point of view.

Therefore, let us consider a gauge-theoretical picture of the HI phase that exits in the EBHM with small particle density. As we explained in the previous works [24], the density fluctuation $\delta\rho_a$ plays a role of an electric field in the gauge theory. Finite $G_{\text{string}}(\ell)$ means that holons and doublons can move rather freely in the sea of the average particle density but their spatial order is such as (\dots , holon, doublon, holon, doublon, \dots), where distances between a holon and adjacent doublons (and a doublon and adjacent holons) are arbitrary. In the gauge theoretical language, doublon and holon correspond to Higgs particle and antiparticle, respectively. The finite string order $\lim_{\ell \rightarrow \infty} G_{\text{string}}(\ell) \neq 0$ means that particle and antiparticle can separate for a large distance, but the above mentioned restriction on the mutual configuration must be satisfied. From the above observation, one can say that the HI state is a *new state* of the gauge theory.

ACKNOWLEDGMENTS

Y.K. acknowledges the support of a Grant-in-Aid for JSPS Fellows (Grant No. JP15J07370). This work was partially supported by a Grant-in-Aid for Scientific Research from Japan Society for the Promotion of Science under Grant No. JP26400246.

-
- [1] I. Bloch, J. Dalibard, and W. Zwerger, *Rev. Mod. Phys.* **80**, 885 (2008); M. Lewenstein, A. Sanpera, and V. Ahufinger, *Ultracold Atoms in Optical Lattices: Simulating Quantum Many-body Systems* (Oxford University Press, Oxford, 2012).
 - [2] O. Dutta, M. Gajda, P. Hauke, M. Lewenstein, D.-S. Luhmann, B. A. Malomed, T. Sowinski, and J. Zakrzewski, *Rep. Prog. Phys.* **78**, 066001 (2015).
 - [3] N. Goldman, G. Juzeliunas, P. Ohberg, and I. B. Spielman, *Rep. Prog. Phys.* **77**, 126401 (2014).
 - [4] G. Jotzu, M. Messer, R. Desbuquois, M. Lebrat, T. Uehlinger, D. Greif, and T. Esslinger, *Nature (London)* **515**, 237 (2014).
 - [5] A. W. Sandvik and J. Kurkijärvi, *Phys. Rev. B* **43**, 5950 (1991); O. F. Syljuasen and A. W. Sandvik, *Phys. Rev. E* **66**, 046701 (2002).
 - [6] E. Altman and A. Auerbach, *Phys. Rev. Lett.* **89**, 250404 (2002).
 - [7] A. J. Daley, J. M. Taylor, S. Diehl, M. Baranov, and P. Zoller, *Phys. Rev. Lett.* **102**, 040402 (2009).
 - [8] S. Diehl, M. Baranov, A. J. Daley, and P. Zoller, *Phys. Rev. Lett.* **104**, 165301 (2010).
 - [9] S. Diehl, M. Baranov, A. J. Daley, and P. Zoller, *Phys. Rev. B* **82**, 064510 (2010).
 - [10] Y.-C. Chen, K.-K. Ng, and M.-F. Yang, *Phys. Rev. B* **84**, 092503 (2011).
 - [11] E. Berg, E. G. Dalla Torre, T. Giamarchi, and E. Altman, *Phys. Rev. B* **77**, 245119 (2008).
 - [12] I. Affleck, *J. Phys. Condens. Matter* **1**, 3047 (1999).
 - [13] T. Kennedy and H. Tasaki, *Phys. Rev. B* **45**, 304 (1992).
 - [14] D. Rossini and R. Fazio, *New J. Phys.* **14**, 065012 (2012).
 - [15] G. G. Batrouni, V. G. Rousseau, R. T. Scalettar, and B. Gremaud, *Phys. Rev. B* **90**, 205123 (2014).

- [16] E. G. Dalla Torre, E. Berg, and E. Altman, *Phys. Rev. Lett.* **97**, 260401 (2006).
- [17] M. Fattori, G. Roati, B. Deissler, C. D’Errico, M. Zaccanti, M. Jona-Lasinio, L. Santos, M. Inguscio, and G. Modugno, *Phys. Rev. Lett.* **101**, 190405 (2008); S. Müller, J. Billy, E. A. L. Henn, H. Kadau, A. Griesmaier, M. Jona-Lasinio, L. Santos, and T. Pfau, *Phys. Rev. A* **84**, 053601 (2011).
- [18] T. Lahaye, C. Menotti, L. Santos, M. Lewenstein, and T. Pfau, *Rep. Prog. Phys.* **72**, 126401 (2009); M. A. Baranov, M. Dalmonte, G. Pupillo, and P. Zoller, *Chem. Rev.* **112**, 5012 (2012).
- [19] S. Inouye, M. R. Andrews, J. Stenger, H.-J. Miesner, D. M. Stamper-Kurn, and W. Ketterle, *Nature (London)* **392**, 151 (1998); C. Chin, R. Grimm, P. Julienne, and E. Tiesinga, *Rev. Mod. Phys.* **82**, 1225 (2010).
- [20] S. Baier, M. J. Mark, D. Petter, K. Aikawa, L. Chomaz, Z. Cai, M. Baranov, P. Zoller, and F. Ferlaino, *Science* **352**, 201 (2016).
- [21] S. Ejima, F. Lange, and H. Fehske, *Phys. Rev. Lett.* **113**, 020401 (2014).
- [22] E. L. Pollock and D. M. Ceperley, *Phys. Rev. B* **36**, 8343 (1987).
- [23] A. W. Sandvik, *Phys. Rev. B* **56**, 11678 (1997).
- [24] Y. Kuno, S. Sakane, K. Kasamatsu, I. Ichinose, and T. Matsui, [arXiv:1605.00333](https://arxiv.org/abs/1605.00333) [Phys. Rev. D (to be published)].
- [25] F. D. M. Haldane, *Phys. Lett. A* **93**, 464 (1983); *Phys. Rev. Lett.* **50**, 1153 (1983).
- [26] By the Holstein-Primakoff transformation with spin S , the bosonic operator is related to spin operators as $S_i^+ = \sqrt{2S - b_i^\dagger b_i} b_i$, $S_i^- = b_i^\dagger \sqrt{2S - b_i^\dagger b_i}$, and $S_i^z = S - b_i^\dagger b_i$. Without taking the large- S limit, the EBHM does not correspond to a simple Heisenberg model because the higher-order terms of b_i and b_i^\dagger appearing from the $1/S$ expansion of S_i^+ and S_i^- lead to complicated interaction terms of bosons, which do not correspond to the on-site nor nearest-neighbor interaction terms of the EBHM.